Line shape analysis of two-dimensional infrared spectra

Qi Guo, Philip Pagano, Yun-Liang Li,[a] Amnon Kohen, and Christopher M. Cheatum[b]
Department of Chemistry, University of Iowa, Iowa City, Iowa 52242, USA and Optical Science and Technology Center, University of Iowa, Iowa City, Iowa 52242, USA

Ultrafast two-dimensional infrared (2D IR) spectroscopy probes femtosecond to picosecond time scale dynamics ranging from solvation to protein motions. The frequency-frequency correlation function (FFCF) is the quantitative measure of the spectral diffusion that reports those dynamics and, within certain approximations, can be extracted directly from 2D IR line shapes. A variety of methods have been developed to extract the FFCF from 2D IR spectra, which, in principle, should give the same FFCF parameters, but the complexity of real experimental systems will affect the results of these analyses differently. Here, we compare five common analysis methods using both simulated and experimental 2D IR spectra to understand the effects of apodization, anharmonicity, phasing errors, and finite signal-to-noise ratios on the results of each of these analyses. Our results show that although all of the methods can, in principle, yield the FFCF under idealized circumstances, under more realistic experimental conditions they behave quite differently, and we find that the centerline slope analysis yields the best compromise between the effects we test and is most robust to the distortions that they cause. © 2015 AIP Publishing LLC. [http://dx.doi.org/10.1063/1.4918350]

I. INTRODUCTION

Two-dimensional infrared (2D IR) spectroscopy is an established third order, nonlinear spectroscopic technique for studying structural dynamics in condensed phases.[1,2] 2D IR probes the time dependent frequency evolution of an ensemble of oscillators to report structural dynamics on time scales ranging from hundreds of femtoseconds to tens of picoseconds. Because the vibrational energy level spacing of an oscillator in a molecule depends on interactions with the environment, time-dependent structural evolution of the environment will alter the vibrational energy-level spacings of the oscillator, which is called spectral diffusion. The evolution of the 2D IR line shape reveals this spectral diffusion. In this way, 2D IR has been applied to study the dynamics of water,[3–6] hydrogen bonded complexes,[7–13] and biological systems such as polypeptides,[14–18] proteins,[19–29] and DNA oligomers.[30,31] A central challenge for this method in all of these applications is how to accurately obtain the parameters that characterize the spectral diffusion process.

The frequency-frequency correlation function (FFCF) is a quantitative representation of the amplitudes and time scales of the frequency fluctuations of an oscillator. The FFCF is defined to be the ensemble average of the product of the frequency fluctuations at time t with those at time zero,

$$C(t) = \langle \delta\omega(t)\,\delta\omega(0)\rangle, \tag{1}$$

where $\delta\omega(t) = \omega(t) - \langle\omega\rangle$. Within the second cumulant approximation, the FFCF is the central quantity used to calculate the 2D IR spectral lineshape function, making it the link between experimental observables, i.e., the 2D IR spectra and the molecular dynamics of the solvation environment around an oscillator. Many approaches have been developed to simplify the extraction of the FFCF from experimental data,[10,32–39] but there is no consensus about which of these methods is most effective or under what circumstances any should be preferred over others.

Researchers have exploited many features to describe the tilt of the diagonally elongated 2D IR lineshape as a function of waiting time, which reflects frequency correlations that are related to the magnitude of the FFCF. The nodal slope, which uses the slope of the nodal contour between the ground-state bleach and excited-state absorption features in the 2D IR spectrum as a metric for the FFCF, was among the first ways of extracting spectral diffusion information from 2D spectra.[10,11,32,39] In 2004, Asbury et al. suggested that the linewidth for a fixed value of ω_3, which they defined as the dynamical linewidth, is related to the FFCF. In 2006, Lazonder et al. proposed an analysis of the ellipticity (ELP) of the 2D lineshape, which is given by a ratio of the sum and difference of the spectral widths along the diagonal and antidiagonal axes, to determine the FFCF.[33] Roberts et al., in 2006, defined two new metrics for the FFCF, the inhomogeneity index, which is the ratio of the difference of the amplitudes of rephasing and nonrephasing spectral features, and the slope of the phase of complex valued 2D correlation spectrum.[34] Their work also evaluated the accuracy of several metrics for the FFCF including the peak shift, the phase slope, the ellipticity, the inhomogeneity index, and the dynamical linewidth, all of which they show can be formally related to the FFCF within a short-time approximation. Their analysis compared the loss of frequency correlations reported by each of these methods to a model FFCF used to simulate the 2D spectra assuming finite laser pulse duration and without making the

---

[a] Current address: Institute of Physics, Chinese National Academy of Sciences, Beijing, China.
[b] Author to whom correspondence should be addressed. Electronic mail: christopher-cheatum@uiowa.edu

short-time approximation. They conclude that all of these methods exhibit some deviations from the actual correlation function for simulated spectra. The dynamical lineshape, in particular, exhibited decays that were too rapid regardless of the form of the correlation function, and was the poorest metric for the model FFCF. Among the other methods that they tested, the deviations from the model FFCF varied depending on the form of the FFCF chosen. Nevertheless, all of these showed good qualitative agreement with the model FFCF and, most importantly, exhibited decays on timescales consistent with the model function. Although all of these methods showed consistency with the model FFCF, their ease of implementation with experimental data differs, and, of these methods, only the ellipticity has seen widespread applications.

More recently, the Fayer group introduced two closely related approaches for extracting the FFCF from 2D IR line-shapes, the inverse centerline slope (IvCLS) and the centerline slope (CLS) methods. They first developed the inverse centerline slope,[35] in which a line is constructed by finding the location of the peak maximum (or minimum depending on whether reporting in absorbance or transmittance) in ω_1 for slices of the 2D spectrum at fixed values of ω_3. The inverse centerline slope is the reciprocal of the slope of the line so constructed. Not only they do show that this method accurately reproduces the model FFCF in simulated data but also demonstrate that it is robust against Fourier filtering methods or apodization. Subsequently, they presented the centerline slope method,[36] which is an improvement on the previously described method that exchanges the roles of the two axes. This development was motivated by the fact that the inverse centerline slope can be affected by interference between the ground-state bleaching and excited-state absorption signals when the anharmonicity is small, and the centerline slope method overcomes this problem. Recent works from Neil Hunt and coworkers have applied a 2D Gaussian fit to the 0-1 transition peak and used the 2D correlation coefficient to report the FFCF.[37] This approach builds on earlier methods that employed Gaussian and short-time approximations as they all start from a 2D Gaussian lineshape. In this approach, a 2D fit to that lineshape directly yields a correlation parameter that is proportional to the FFCF.

The goal of this paper is to test the robustness of methods for extracting the FFCF from experimentally measured 2D IR spectra. We have chosen to test only the most commonly used analysis methods and those with established robustness to key experimental distortions. Specifically, we compare the CLS, the IvCLS, the ELP, the nodal line slope (NLS), and the 2D Gaussian correlation (2DGC) methods to assess their robustness against some common factors encountered in real experiments—apodization, anharmonicity, and finite signal-to-noise ratio (S/N).

Apodization or windowing is a necessary consequence of discrete sampling and is implicitly or explicitly a part of all experimental spectral measurements. A time/frequency axis is necessarily windowed both by a finite measurement length and data interval and either an implicit or explicit windowing function. In 2D IR, specifically, the most commonly employed experimental approaches measure the ω_3 axis in the frequency domain using a spectrometer, which implicitly apodizes the ω_3 axis with a square windowing function. In contrast, the ω_1 axis is measured as an interferogram in the time domain. The length of time over which this measurement is made is the apodization time, and the interferogram is typically multiplied by a simple windowing function to take the data smoothly to zero before Fourier transformation into the frequency domain. In some cases, it can be advantageous to reduce the apodization time as the choice of apodization time determines the time it takes to collect a spectrum. For rapid data acquisition or in the case of samples where the signals are weak and significant data averaging may be required, choosing a shorter apodization time can greatly decrease the measurement time. The choices of apodization time and function, however, will impact the spectral lineshape in the frequency domain. We address the question of the extent to which the apodization time and function affect the extraction of the FFCF using the aforementioned methods.

Anharmonicity is another characteristic that varies from system to system and can affect the ability of a particular analysis method to retrieve the FFCF accurately. If the anharmonicity is small relative to the width of the 2D lineshapes for the 0-1 and 1-2 transitions, then these oppositely signed spectral features will interfere. This interference can distort the 2D IR lineshape and influence the ways that some of the analysis methods are able to extract information about the frequency correlations. As noted already, Kwak *et al.* demonstrated that the IvCLS method exhibits significant deviations from the known FFCF for simulated data in which the anharmonicity is too small.[36] In contrast, if the anharmonicity is large compared to the linewidth, then the peaks will be well separated. Although, for most methods, this separation is expected to be advantageous as it minimizes distortions of the lineshape, it may well have a deleterious effect on the NLS method because the node will be located in the empty spectral region between the peaks where noise dominates and can significantly alter the shape of the nodal contour.

Although the developments of pulse shaping technologies[40] and methods to measure and correct the phase difference between pulses in four-wave mixing experiments[41] have provided the means to essentially eliminate phasing errors in 2D IR spectra, research groups have been slow to adopt these methods, and many groups still correct the phasing errors using the projection-slice theorem in post processing. As a result, small phasing errors can still remain in the data resulting from the relative insensitivity of the pump-probe projection to small phasing errors and the weakness of the pump-probe spectrum in an apparatus designed to measure four-wave mixing spectra. These small phasing errors appear as an error in the value of the zero delay time either for the time delay between the first two pulses or the time delay between the third pulse and the local oscillator. This introduces a group delay error, which corresponds to a frequency dependent phase shift that introduces a small dispersive contribution to what is normally a purely absorptive correlation spectrum. We show that the resulting phase twist will distort the lineshape and affect the analysis of the lineshape to extract the correlation decay.

Finally, every experimental measurement will be limited by the finite signal-to-noise ratio of the data. Previous studies comparing the accuracy of the various methods for extracting the FFCF from the 2D IR data have all done so in the

context of simulated 2D IR spectra with essentially infinite S/N. These studies focused on the question of which method was most accurate. In this study, we address the more practical consideration of which method will be the most robust in the face of realistic noise on the experimentally measured data. Particularly in the case of biological samples, where the concentration of the analyte is limited, the S/N levels can be quite modest making the choice of analysis method potentially critical to the success or failure of the experiment. We show that, indeed, there are considerable differences in the ability of each of the studied methods to extract the correlation information when the S/N ratio becomes poor, and that, ultimately, the CLS method offers the best compromise of the impacts of the studied effects.

II. METHODS

A. Data simulation

We follow the derivations of a three level system of anharmonic oscillators described in Ref. 1. Briefly, we assume a simple Kubo model for the FFCF,

$$C(t) = \Delta_1^2 + \Delta_2^2 e^{-t/\tau_2}, \tag{2}$$

where the Δ's represent the magnitudes of the frequency fluctuations of the oscillator being probed and τ_2 reports the spectral diffusion time scale. This correlation function gives a lineshape function, $g(t)$, of the form,[1,42]

$$g(t) = \Delta_1^2 \frac{t^2}{2} + \Delta_2^2 \tau_2^2 \left(e^{-\frac{t}{\tau_2}} + \frac{t}{\tau_2} - 1 \right). \tag{3}$$

We can write the form of the rephasing and nonrephasing response functions as R_r and R_{nr}, respectively. These response functions account for the population lifetime, T_1, in addition to the aforementioned lineshape function, $g(t)$, and are written as

$$
\begin{aligned}
R_r &= \exp\left(-i \times \omega_0 \times (-t_1 + t_3)\right) \\
&\quad \times \exp\left(-g(t_1) + g(T) - g(t_3) - g(t_1 + T)\right. \\
&\quad - g(T + t_3) + g(t_1 + T + t_3)\right) \\
&\quad \times \left(2 \exp\left(\frac{-(t_3 + 2T + t_1)}{2T_1} \right) \right. \\
&\quad - 2 \exp\left(\frac{-(3t_3 + 2T + t_1)}{2T_1} \right) \times \exp\left(-i \times A \times t_3\right) \right),
\end{aligned}
\tag{4}
$$

$$
\begin{aligned}
R_{nr} &= \exp\left(-i \times \omega_0 \times (t_1 + t_3)\right) \\
&\quad \times \exp\left(-g(t_1) - g(T) - g(t_3) + g(t_1 + T)\right. \\
&\quad + g(T + t_3) - g(t_1 + T + t_3)\right) \\
&\quad \times \left(2 \exp\left(\frac{-(t_3 + 2T + t_1)}{2T_1} \right) \right. \\
&\quad - 2 \exp\left(\frac{-(t_3 + 2T + t_1)}{2T_1} \right) \times \exp\left(-i \times A \times t_3\right) \right),
\end{aligned}
\tag{5}
$$

TABLE I. Parameters used for simulated 2D IR spectra.

Δ_1 (ps^{-1})	Δ_2 (ps^{-1})	τ_2 (ps)	T_{pop} (ps)	A (cm^{-1})
0.3	1.4	1.3	1.3	25

where ω_0 is the average transition frequency of the oscillators, A is the anharmonicity, t_1 is the time delay between the first two electric field interactions, t_3 is the time after the third electric field interaction, T is the waiting time between the second and third electric field interactions, and T_1 is the population lifetime.

Following the equations above, we use the parameters in Table I to generate the time domain response functions using MATLAB (R2012a, The Mathworks, Inc.). The parameters are approximately those for azide in D$_2$O consistent with the experimental measurements reported by Hamm *et al.*,[9] which also contained a shorter time scale decay of 80 fs associated with $\Delta = 2.6$ ps^{-1} that we neglect for simplicity and to avoid having to sample waiting times short enough to resolve this component of the decay. Thus, we include only the longer time scale decay of 1.3 ps associated with an amplitude of $\Delta_2 = 1.4$ ps^{-1} and the static off set $\Delta_1 = 0.3$ ps^{-1}. Together these amplitudes correspond to relative amplitudes of 0.96 and 0.04 for the decay and the static components, respectively. The time domain data, a matrix of intensity for each (t_1, t_3) pair is exported for further data manipulation and analysis.

We import the time-domain simulated data, both rephasing and nonrephasing, into IGOR Pro (version 6.36, Wavemetrics, Inc.) and multiply each by a windowing function of the form,

$$win = \cos\left(\frac{x \cdot \pi}{2l} \right) \cos\left(\frac{y \cdot \pi}{2w} \right), \tag{6}$$

where l is the number of points for the t_1 axis and w for t_3. This cosine windowing function has the effect of smoothly taking the time domain signal to zero regardless of the length of time over which we have calculated the response. The windowed response function is zero-padded and Fourier transformed to generate the complex-valued, frequency-domain response functions. Taking the real parts of the complex-valued spectra and rotating them into the same quadrant in the 2D frequency space, we sum them together to get the 2D correlation spectrum, which is the conventional representation of the 2D IR spectrum. To address the effects of apodization function, we also use the following two windowing functions:

$$win = \left(1 - \frac{x}{l} \right) \cos\left(\frac{y \cdot \pi}{2w} \right) \tag{7}$$

and

$$win = \sqrt{2} \sin\left(\frac{3 \cdot \pi \cdot x}{4l} + \frac{\pi}{4} \right) \cos\left(\frac{y \cdot \pi}{2w} \right), \tag{8}$$

which we refer to as the triangle and shifted sine-bell functions, respectively. The triangle windowing function takes the free induction decay (FID) to zero more rapidly than the cosine windowing function. In contrast, the shifted sine-bell function enhances the signal from the middle portion of the FID before smoothly going to zero, effectively extending the time over which the FID decays somewhat.

To study the effect of apodization time, we vary the maximum value of t_1, the first coherence time, when generating the time domain data. Experimentally, most labs use array detectors for data collection in the frequency domain, and t_3 is directly apodized and Fourier transformed by the spectrometer to produce frequency domain data in ω_3. In contrast, most experiments measure the spectral response as a function of excitation frequency in the time domain meaning that they must choose an apodization time and an apodization function just as we have for the simulated data. To be most consistent with the common experimental approach, we leave the apodization time and windowing function for the detection frequency, ω_3, unchanged, whereas we vary the apodization time systematically for the excitation frequency by changing the maximum value of t_1 for which we simulate the data and windowing according to Eqs. (6)–(8) followed by Fourier transformation to get the spectral response as a function of ω_1 for each value of ω_3. We start with a simulated coherence time that is typical for such experiments and allows for the measurement of the interferogram to a point where the signal has nearly fully decayed, 4 ps. We vary this value to shorter coherence times to a smallest value of 1 ps, which is much shorter than the timescale for decay of the interferogram.

To assess the effects of anharmonicity, we change the magnitude of the anharmonicity parameter, A, from a value that is small compared to the experimental line width, 5 cm^{-1}, to a value that is large compared to the line width, 53 cm^{-1}. These values are consistent with the physically reasonable range of observable anharmonicities for high frequency molecular vibrations.

To determine the effects of phasing errors, we multiply the complex valued response functions for the rephasing and non-rephasing pathways, after the double Fourier transformation, by a frequency dependent phase factor of the form,

$$Phase\ Error = \exp\left(i \cdot \Delta t \cdot 2 \cdot \pi \cdot c \cdot \omega_3\right), \qquad (9)$$

where Δt is the phase error and ω_3 is the frequency variable that is the Fourier conjugate of the t_3 axis. We choose this form for the phase error because the error in setting time zero between the local oscillator and the third pulse in 2D IR measurements is often the largest source of phase error. Although phasing errors do not appear in experiments using a pulse shaper such as in our measurements, they are a potential source of distortions in four-wave mixing experiments, which are still quite common. Though we could introduce such phase errors in a number of forms, this type of phasing error, i.e., a frequency dependent phase shift arising from a group delay associated with incorrectly determining the zero delay between two pulses, illustrates the distortions of phasing errors adequately to assess the effects of those distortions on the analysis of 2D IR lineshapes. Because this phasing error is intended to model a small group delay error in t_3, we apply the same phase error to both the rephasing and nonrephasing spectra.

B. Experimental methods

The 2D IR pulse-shaping apparatus is similar to that reported previously.[27] Briefly, a commercial Ti: sapphire laser with a repetition rate of 1 kHz produces pulses of ∼90 fs duration centered at 800 nm with a per pulse energy of ∼4 mJ. Approximately, 1200 μJ/pulse of the reflected light pumps a home-built two-pass optical parametric amplifier (OPA) based on a β-barium borate (BBO) crystal (θ = 27°, type II). The energy difference between the signal and idler beams from the OPA is tunable, and we adjust this difference to the desired mid-IR frequency, ∼2040 cm^{-1}. Difference frequency generation (DFG) of the signal and idler in a AgGaS$_2$ crystal (θ = 50°, type II) produces ∼5 μJ mid-IR pulses that are ∼120 fs in duration with a full width at half-maximum (FWHM) of ∼180 cm^{-1}. The pulse-shaper apparatus produces a 2D IR spectrum in a pump-probe experimental geometry. The shaped pump beam provides the first two electric-field interactions, and the probe beam is the last electric-field interaction and the local oscillator. We detect the signal using the CMOS array detector after upconversion of the probe beam cycling the pulse shaper through a sequence of masks that vary the relative phases (0,0; 0,π; π,0; π, π) and the time delays between the two pump pulses from 0 to 4 ps in 24 fs steps, from which we can reconstruct the time-frequency data. These data are windowed using the same windowing function as for the simulated data in Eq. (6) and Fourier transformed yielding the 2D frequency spectrum for a given waiting time. A sample containing 50 mM azide in D$_2$O is held between calcium fluoride windows with a 56 μm spacer for 2D IR measurements. All chemicals were purchased from Sigma Aldrich and used without further purification.

C. Line shape analysis

We apply five different methods to analyze the 2D IR lineshapes. Figure 1 illustrates these analysis methods using the simulated data with T = 1600 fs. Panel (a) shows the analysis for the CLS, IvCLS, and NLS. For the CLS, we take slices through the 2D IR spectra at each value of ω_1 and locate the position of the minimum in ω_3, marked as purple dots. The resulting sequence of points is the centerline, and we fit the centerline with a linear function over a small range around the peak center from 2043 to 2048 cm^{-1} in ω_1, which is marked by a solid white line. The slope from this linear fit is the CLS and is recorded for each waiting time T. Similarly for the IvCLS, we take slices at each value of ω_3 and locate the position of the minimum in ω_1, marked as blue dots. The resulting sequence of points forms a different centerline from that of the CLS method, and we fit this centerline with a linear function on a small range around the peak center from 2043 to 2048 cm^{-1} in ω_3, which is again highlighted as a solid white line. In this case, the inverse of the slope from this linear fit is the IvCLS and is recorded for each waiting time T. To get the nodal line, we find the node, or zero value, for each ω_1 slice by finding the minimum and maximum as a function of ω_3 for each value of ω_1. We then fit the data between the maximum and minimum as a function of ω_3 to a sinusoid and find the root of this sinusoid using the built-in FindRoots function in IGOR Pro, which uses Brent's method to find the root for each slice. The resulting sequence of zero-crossing values for each ω_1 slice is the nodal line, shown as red dots in Figure 1(a). We fit the nodal line to a linear function over a small frequency range
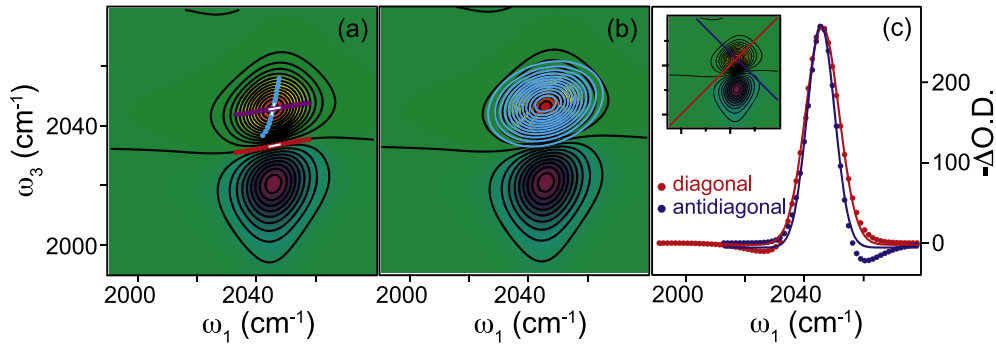
FIG. 1. Illustration of the methods for extracting the FFCF from simulated data with T = 1600 fs. (a) The purple, blue, and red dots represent the centerline, inverse centerline, and nodal line, respectively, and the white solid lines are the corresponding linear fits. (b) The 2D Gaussian fit (solid blue lines) to the 0-1 peak. (c) The diagonal (red dots) and anti-diagonal (blue dots) slices from the 2D spectrum (inset) are shown as data points and the solid lines are the corresponding Gaussian fits.

from 2043 to 2048 cm^{-1} in ω_1, which is shown as a solid white line, and the slope (NLS) is recorded for each waiting time.

For each of the above methods, CLS, IvCLS, and NLS, we apply a linear fit to determine the relevant correlation parameter. In each case, we use a narrow range, ∼5 cm^{-1}, around the center of the transition. The choice of the range over which we make these linear fits can potentially impact the results of the analysis. In the case of the simulated data, this effect is very minor as the centerlines and nodal line are all well modeled by a linear function in the vicinity of the peak maximum. Thus, varying the exact width or location of the fit region has little effect on the slopes that result from the fits with the exception of the effects on the NLS and IvCLS methods due to large and small anharmonicities, respectively, as described in detail later. For the experimental data, the choice of fit region is more sensitive. If the fit region is too small, i.e., less than 3-5 data points, then the inherent noise in experimental data can make the slope an unstable parameter from the fit. If the fit region becomes too large, i.e., when the fit region approaches the edges of the lineshape where noise or interference with the 1-2 transition can distort the lineshape, then the distortions from the edge of the lineshape can affect the quality of the fit. Thus, as a general rule, the fitting region should not extend beyond the FWHM of the diagonal slice of the spectral feature. Within these bounds, the results of the analysis methods that depend on a linear fit to a characteristic feature of the spectrum are robust to minor variations of the width or position. The exception to these guidelines is when the lineshape is curved giving rise to nonlinear behavior for the centerlines or nodal line. In this situation, there is no entirely objective and reliable way to determine how to make a linear fit to the nonlinear functions.

Figure 1(b) shows the 2D Gaussian fit (purple contours) of the 0-1 transition in the simulated data for T = 1600 fs. We do the fitting in IGOR Pro using the built-in 2D Gaussian fitting routine, which has the functional form,

$$Amp = z_0 + a \exp\left[\frac{-1}{2(1-corr^2)}\left(\left(\frac{x-x_0}{\sigma_x}\right)^2 \right.\right.$$
$$\left.\left. + \left(\frac{y-y_0}{\sigma_y}\right)^2 - \frac{2 \cdot corr \cdot (x-x_0)(y-y_0)}{\sigma_x \cdot \sigma_y}\right)\right], \quad (10)$$

where a is the amplitude; z_0 is the baseline offset; x_0 and y_0 are the center frequency positions in ω_1 and ω_3, respectively; σ_x and σ_y are the variances that determine the widths of the peak in ω_1 and ω_3, respectively; and $corr$ is the 2DGC coefficient, which is proportional to the value of the FFCF.

To determine the ELP, we first identify the position of the peak center, and from this position, we extract the diagonal slice where (ω_1, ω_3) pairs obey the relationship $\omega_3 = (\omega_1 - x_0) + y_0$. Similarly, we also construct an anti-diagonal slice where all (ω_1, ω_3) pairs obey the relationship $\omega_3 = -(\omega_1 - x_0) + y_0$. Depending on the sampling interval of the frequency-domain data, it is possible that no data points exist on the diagonal or anti-diagonal slices, so we interpolate the data matrix in the frequency domain to an evenly spaced grid of points with a point spacing of 0.17 cm^{-1}. Figure 1(c) shows the diagonal (red points) and antidiagonal (blue points) slices from the simulated data for T = 1600 fs. We calculate the ELP according to the expression,

$$ELP = \frac{a^2 - b^2}{a^2 + b^2}, \quad (11)$$

where a and b are, respectively, the diagonal and antidiagonal linewidths, σ, that come from fitting the diagonal and antidiagonal slices to Gaussian lineshapes (solid lines).

All of the results of these analysis methods, CLS, IvCLS, NLS, ELP, and 2DGC, are plotted versus the waiting time and can be fit to an analytical expression, typically a sum of exponentials, that is proportional to the full FFCF. To get the FFCF, the amplitude of the function, corresponding to the magnitude of all of the frequency fluctuations, can be obtained through a fit to the FTIR spectrum or a 2D IR spectrum based on the parameters, i.e., relative amplitudes and timescales, of the analytical fitting expression.[35,36]

III. RESULTS AND DISCUSSION

A. Apodization effects

As described above, based on the parameters in Table I, we simulate data and analyze it with different apodization times decreasing from 4 ps to 3 ps, 2 ps, 1.5 ps, and 1 ps and different apodization functions, cosine, triangle, and shifted cosine. For each of the different apodization times, we window the data using the apodization function in Eq. (6), and we
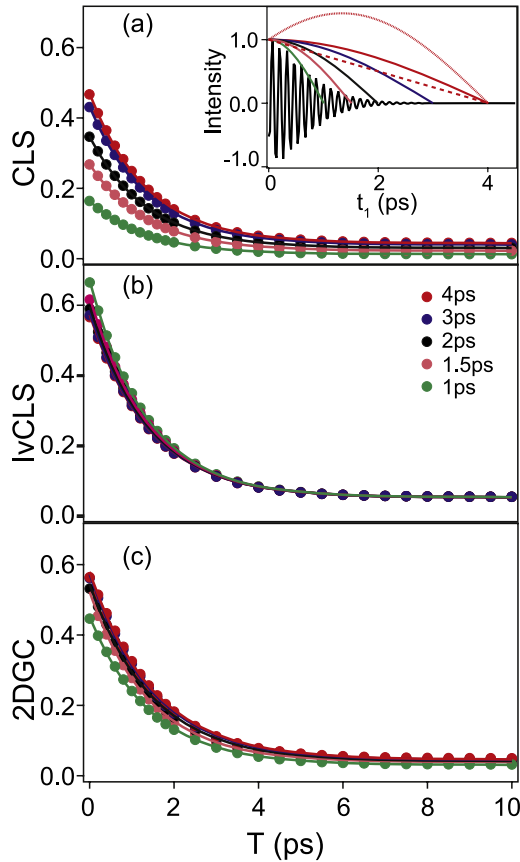
FIG. 2. Apodization effects on (a) CLS, (b) IvCLS, and (c) 2DGC methods. The inset shows the FID as a function of t_1 and the windowing functions for the different apodization functions and times. For each analysis method, markers represent the data points and lines are the single exponential fits to those points. ELP and NLS methods behave similarly to CLS and are presented in the supplementary material.[44]

TABLE II. Single exponential fit parameters for CLS, IvCLS, and 2DGC analyses for different apodization times.

Analysis method	Apodization t_1/ps	A_1	τ/fs	A_2
	4	0.43	1400	0.044
	3	0.39	1400	0.039
CLS	2	0.32	1400	0.030
	1.5	0.25	1400	0.022
	1	0.15	1300	0.013
	4	0.52	1400	0.051
	3	0.53	1400	0.051
IvCLS	2	0.54	1400	0.051
	1.5	0.56	1400	0.052
	1	0.62	1400	0.052
	4	0.53	1500	0.046
	3	0.53	1500	0.045
2DGC	2	0.50	1500	0.041
	1.5	0.42	1400	0.038
	1	0.42	1400	0.030

zero pad the windowed data to a total of 1024 points in the time domain before Fourier transformation to the frequency domain. Because we zero pad all of the data to the same total number of points, the point spacing in the frequency domain will be the same, but the information content of the apodized data sets will decrease as the apodization time decreases reflecting the truncation of the signal. We then apply all five of the analysis methods described above to each of these data sets. Figure 2 shows the results of analysis of the 5 simulated data sets by CLS (a), IvCLS (b), and 2DGC (c). The points are the results of the analyses at each of the individual waiting times, and the solid lines are single exponential fits to these points,

$$Amplitude = A_1 e^{-t/\tau} + A_2, \qquad (12)$$

for which the fitting parameters are summarized in Table II.

The inset in Figure 2(a) illustrates the effect of reducing the apodization time for the time domain data. The black oscillatory trace is a slice of the simulated data as a function of τ_1 for $\omega_3 = 2045$ cm^{-1}. The colored curves show the windowing function for each of the five values of the apodization time ranging from 1 ps at the shortest to 4 ps at the longest. As is clearly evident from this plot, the shorter the apodization time the more of the free-induction decay that will be cut off by the apodization function. Furthermore, the longer apodization times will affect the response less than the shorter apodization

times because only the portion of the free induction decay that already has low amplitude will be affected significantly by the apodization function. Whereas, for shorter apodization times, the apodization function affects the data in a region of time where the signal itself is quite significant. Thus, we would expect that any effect of the apodization on the analysis methods should be modest for the longer apodization times but will increase substantially, almost exponentially, as the apodization time decreases. Although it is possible, in principle, to increase the apodization time so that the windowing function does not significantly affect the free induction decay, it is worth noting that this figure is a simulated result and that for real data, the long coherence time response will be dominated by noise so that there comes a point at which increasing the apodization time does not significantly affect the lineshape but does add noise. Thus, there is a practical limit to how large an apodization time one should choose based on the time scale of the free induction decay.

For the CLS analyses shown in Figure 2(a), the amplitudes of the exponential decay decrease significantly with decreasing apodization time. In contrast to the amplitudes, however, the time constants are essentially unchanged except for the extreme example of a 1 ps apodization time for which the time constant of the fit is shorter by 7%. Thus, although the time constant from the CLS analysis is quite robust to reducing the apodization time, there is a substantial effect on the amplitudes. Of course, because the FFCF is only proportional to the CLS and not equivalent to it, the absolute amplitudes of the CLS decay are much less important than the relative amplitudes, as these are the values that get scaled by fitting to a spectrum to give the full FFCF. The relative amplitudes do vary somewhat as a result of apodization. The ratio $A_2/(A_1 + A_2)$, which is the relative amplitude of the static term, exhibits a decreasing trend from a value of 0.093 for 4 ps apodization time to a value of 0.077 for 1 ps apodization time, all of which overestimate the relative amplitude of the static component compared to its relative amplitude in the FFCF of 0.04. The variation in the static component means that there is a corresponding increase

in the relative amplitude of the exponential decay term from 0.907 to 0.923. This variation corresponds to a roughly 20% change in the value of the static component, which is on the order of the size of the uncertainty in the value of the relative amplitude of the static component in most experiments. Obviously, this effect is proportionately smaller for the exponential decay term. Thus, although there is some effect on the relative amplitudes, we conclude that this effect is sufficiently modest that under realistic experimental conditions, it would be less than the measurement uncertainty in the values and can, therefore, be neglected. The data for the analysis using NLS and ELP methods are not shown here (see supplementary material[44]) but the behavior of these methods is remarkably similar to that for the CLS and the same conclusions can reasonably be made about the effects of apodization time for these methods.

Figure 2(b) shows the analyses of the data for different apodization times using the IvCLS method. In this case, the data points for the different apodization times fall almost exactly on top of one another even for the shortest apodization time of 1 ps. This demonstrates that the IvCLS method is very robust against changes in the apodization, which is consistent with the findings from Kwak *et al.* in the manuscript where they introduced the IvCLS approach.[35] This robustness to apodization is the major advantage of the IvCLS method, but as already demonstrated by the Fayer group and as we show again below, this method suffers from other failings that can make it unsuitable. Nevertheless, for systems where it is suitable, it remains an attractive method as a result of this feature.

Figure 2(c) shows the analyses for the 2DGC method. Clearly, the 2DGC is much more robust to changes in the apodization time than the CLS though not quite to the extent of the IvCLS. In addition, apodization time has a greater effect on the amplitude of the exponential decay than on the offset and again has very little effect on the time constant. Clearly, the relative amplitudes will not be constant, but the variations in the amplitude are sufficiently small that it is unlikely that they would be observable in a real experiment.

In addition to assessing the effects of changing the apodization time for the cosine windowing function in Eq. (6), we have also tested the effects of changing the apodization function itself by using the windowing functions in Eqs. (7) and (8), the triangle and shifted sine-bell functions, respectively (data shown in the supplementary material[44]). Based on the effects of apodization time, however, the effects of apodization function are completely intuitive. The inset in Figure 2 shows the apodization functions along with the FID as a function of t_1. The three windowing functions in red are the triangle, cosine, and shifted sine-bell functions, where the triangle is dashed and shifted sine-bell is the only function with an amplitude greater than 1 at any point. Multiplying each of these functions by the FID will have predictable effects relative to the cosine function. The triangle function decays more rapidly than the cosine function for the same apodization time. This effect will cause the windowed FID to decay more rapidly, just as if we had used the same windowing function for a shorter apodization time. In contrast, the shifted sine-bell function increases the amplitude of the FID at intermediate times stretching the time scale over which the windowed FID decays. Thus, the triangular function

apodizes more aggressively than the cosine does and the shifted sine-bell function apodizes less aggressively. Consistent with our results for apodization time, these changes have different effects depending on the analysis method. For the IvCLS method, the apodization function, like the apodization time, has no effect. For the CLS, ELP, and NLS methods, the amplitude of the decay in each case depends on the degree of apodization with more aggressive apodization corresponding to smaller amplitudes and less aggressive apodization to larger amplitudes, but the time constants are unperturbed in each case. For the 2DGC method, the effects are intermediate between those for the IvCLS and the other methods. Thus, the effect of changing the apodization function from less to more aggressive apodization is qualitatively similar to that for reducing the apodization time.

All of the above discussion centers on the effects of apodization in the ω_1 axis, which we collect in the time domain. As already noted, the apodization in the ω_3 axis is, most often, implicit as this spectral dimension is collected directly in the frequency domain, most often using an array detector, and the implicit rectangular apodization function is a constant that is characteristic of the apparatus and determined by the resolving power of the spectrometer, the entrance slit width, and the pixel pitch of the array. In our experimental apparatus, we upconvert and detect the signal in our experiment using a relatively high pixel density (1024 pixels) CMOS array, many labs use MCT array detectors, which have significantly lower pixel densities (128 pixels), to detect directly in the IR. Thus, the implicit apodization functions in the ω_3 axis will be different for these two detection systems. Specifically, the higher pixel density of the upconversion approach will give rise to a narrower rectangular windowing function in the frequency domain than for the MCT array detector depending on the resolution element of the spectrometer. Nevertheless, although these differences will affect the absolute amplitudes of the decays in ways that are similar to those reported for the ω_1 axis above, because the apodization is the same for all measurements, it will not affect the relative amplitudes or the time constants of those analyses. In addition to the difference in pixel density, the upconversion apparatus could also limit the detection bandwidth depending on the phase-matchable bandwidth of the upconversion crystal, which could distort the lineshape for very broad transitions such as for the O–H stretch of water. In practice, it is relatively easy to choose a crystal thickness such that the phase-matchable bandwidth of the upconversion step far exceeds the bandwidth of the IR laser pulses used for the experiment even when using very short and thus very broad laser pulses. Consequently, this potential source of distortion should not be an issue if the crystal thickness is chosen appropriately. Thus, although there can be differences in implicit apodization in ω_3, these differences should not affect the trends we have reported.

Apodization changes in ω_1 have little effect on the decay time for any of the analysis methods. If one only cares about the FFCF decay time, then any of the analysis methods will be suitable for any apodization time. The most important feature, however, is that the apodization time will affect the amplitude of the correlation as reported by most of the analysis methods. Thus, although the apodization time is an experimental choice,

once it has been made it must remain the same for all waiting times. The only exception is if the data will be analyzed by the IvCLS, which is entirely unaffected by apodization in the first coherence period.

B. Anharmonicity effects

The anharmonicity of the oscillator is a characteristic feature of the vibrational mode being studied that determines the spacing between the 0-1 and the 1-2 transitions in ω_3. The anharmonicity of an oscillator can affect the observed lineshapes whenever it is small compared to the width of the transitions. In this case, the oppositely signed 0-1 and 1-2 features will destructively interfere distorting the line shape in the region where they overlap. These distortions might well be expected to affect the ability of different analysis methods to accurately extract the correlation dynamics. For well-separated peaks where the anharmonicity is larger than the line width and there is no interference, the line shapes are undistorted, but, as presented below, some analysis methods may still be unsuitable. Here, we systematically vary the anharmonicity to assess the effects of interference between the peaks, or lack thereof, on the line shapes and the line shape analysis. We simulate three sets of data using the parameters in Table I with an apodization time of 4 ps and varying the anharmonicity, A, from 5, to 25 to 53 cm^{-1}. We apply all five analysis methods to the three data sets (Figure 3) and fit the results with a single exponential decay as before (Table III).

Figure 3(a) shows the results of the CLS analyses for the three anharmonicity values. As would be expected, the CLS is insensitive to the interference that distorts the lineshape for small anharmonicities. This feature is, in fact, one of the main motivations for developing this approach when it was first reported. Similar to the CLS, the ELP method is insensitive to changes in the lineshape caused by small anharmonicities though unlike the CLS, there are modest perturbations to the amplitudes of the decay for this method (see supplementary material[44]). These methods are both resistant to the effects of the interference between the peaks because they rely on portions of the spectrum that are not significantly distorted by those interferences. The CLS locates the maximum of the peak in ω_3, which is always in the central region of the peak. The ELP extracts the diagonal and anti-diagonal slices, which are not directly affected by the interference between the peaks.

In contrast, Figure 3(b) shows the IvCLS results for which these distortions have a significant impact. Although the impact of the interference that results from the 25 cm^{-1} anharmonicity is modest, the 5 cm^{-1} result deviates considerably from the unperturbed spectrum, i.e., the 53 cm^{-1} anharmonicity. The effects of this distortion are seen in the inset. The centerline exhibits a distinct curvature where the 0-1 and 1-2 transitions interfere. This problem was noted by the Fayer group and is the major reason that this method is not more widely used since systems where the anharmonicity is small compared to the line width are fairly common. Somewhat surprisingly, the 2DGC method shows a similar trend to what is seen for the IvCLS (see supplementary material[44]). Although the magnitude of the effect is less, the distortions caused by the overlapping peaks cause the 2D Gaussian fit to converge with
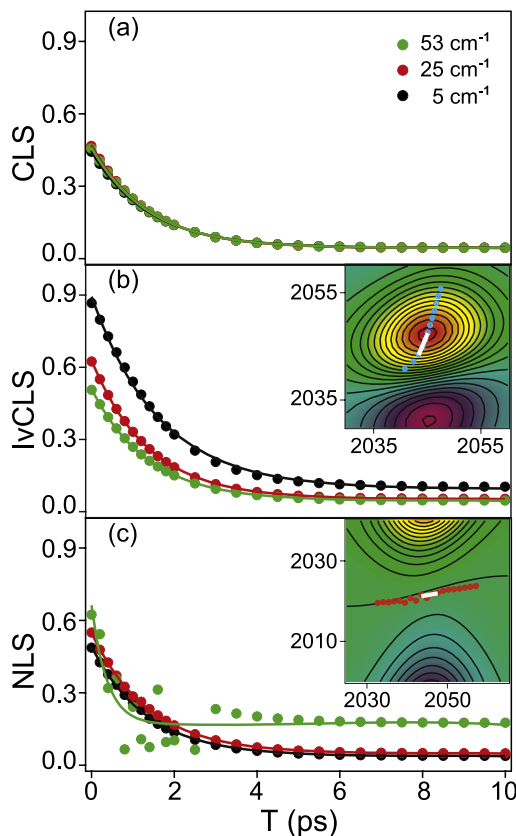

FIG. 3. CLS (a), IvCLS (b), and NLS (c) analyses for simulated data with anharmonicities of 53 (green), 25 (red), and 5 cm^{-1} (black) anharmonicities. The dots are the results of the analyses at each waiting time and the lines are the result of single exponential fits to the decays. The insets in (b) and (c) show spectra for T = 1600 fs, illustrating the distortions that arise in the IvCLS (b) and NLS (c) methods for small and large anharmonicities, respectively.

a consistently higher correlation term than is present for the unperturbed case. In addition, the time constant systematically increases with decreasing anharmonicity. In both of these cases, the problem is that the analysis methods are significantly dependent on the region where the two peaks interfere. In the case of the IvCLS, it is possible to only analyze the portion of the spectrum for high ω_3, but this region of the spectrum will be more significantly affected by noise, which will be exacerbated by the fact that we will be fitting the centerline over a smaller range to avoid the overlap region. For the 2DGC

TABLE III. Single exponential fit parameters for CLS, IvCLS, and 2DGC analyses for different anharmonicities.

Analysis method	A/cm^{-1}	A_1	τ/fs	A_2
	53	0.42	1400	0.044
CLS	25	0.43	1400	0.044
	5	0.40	1400	0.044
	53	0.46	1300	0.045
IvCLS	25	0.52	1400	0.051
	5	0.80	1500	0.094
	53	0.50	380	0.17
NLS	25	0.50	1400	0.048
	5	0.45	1400	0.037

method, the fitting routine needs to fit a 2D Gaussian to the entire lineshape. The interference between the two spectral features distorts this lineshape moving the apparent center frequency higher in ω_3 and flattening out the 0-1 peak along the diagonal, which is responsible for the increase in the 2DGC values for small anharmonicities. It is clear that, in general, the qualities of the 2D Gaussian fits to the data are poorer for small anharmonicities suggesting that the spectral distortions are a significant problem for this analysis method.

In contrast to all of the other methods, the NLS approach shows the poorest behavior for the largest anharmonicity and the best behavior for the smallest anharmonicity. Figure 3(c) shows the NLS results. The black and red represent the NLS analyses for 5 and 25 cm^{-1} anharmonicities, respectively. These two decays are consistent with the FFCF used to simulate the spectra. For the largest anharmonicity of 53 cm^{-1}, however, the NLS analysis becomes unstable as seen in the inset. Recall that the NLS method relies on identifying the node, the zero value between the peaks, for each ω_1 slice. For small anharmonicities compared to the lineshape, the resulting interference between the peaks ensures that the node occurs in a region where the signal contributions from both the 0-1 and the 1-2 peaks are large. The node occurs only because of the interference between these two oppositely signed contributions. Thus, the node is in a region of the spectrum where the signal is high. For large anharmonicities, however, there is a region of no signal in between these two spectral features, and the node will be located somewhere in this empty spectral region where there is no signal (see inset). In this situation, even extremely small perturbations can have a significant effect on the nodal slope. As Figure 3(c) shows, the NLS method, when applied to data with large anharmonicity, fails even for simulated data. Although this method will be quite suitable when the anharmonicity is small compared to the line width, for larger anharmonicities, it is clear that this method is inappropriate.

C. Phasing effects

Although pulse shaping measurements of 2D IR spectra based on a pump-probe geometry are inherently properly phased and recently developed methods can eliminate phasing errors even in four-wave mixing spectra, many researchers still employ the projection-slice theorem to correct the phasing errors that inherently arise from the uncertainty in setting the zero delays between the first and second pulses and between the third pulse and local oscillator when measuring 2D IR spectra using a spectrometer based on four-wave mixing. This uncertainty in the zero delay between pulses corresponds to a group delay and gives rise to a frequency dependent phase shift. As a result of this frequency dependent phase, differing amounts of the dispersive contribution to the lineshape will get mixed into the absorptive lineshape at each frequency in both the rephasing and nonrephasing spectra, and there will be inexact cancelation of these dispersive contributions when the two component spectra are summed to give the correlation spectrum. The result will be that the correlation spectrum will have a lineshape that still contains some phase twist that

is dependent on the frequency along the axis corresponding to the uncorrected phase error. The projection-slice theorem is used to correct this phase error by adjusting the phase of the rephasing and nonrephasing spectra such that the integral of the 2D IR correlation spectrum over the ω_1 axis gives a signal that exactly corresponds to the dispersed pump-probe spectrum for the same waiting time. Although this method offers a mechanism to correct the phasing errors, it is rather insensitive to small phasing errors that, while small enough to have little effect on the pump-probe projection, can still significantly distort the 2D IR lineshape.

To test the effects of phasing errors on the analyses of the 2D IR lineshapes, we have simulated spectra where we multiply the rephasing and nonrephasing spectra by a frequency-dependent phase factor of the form given in Eq. (9). We have chosen to apply the phase factor to the ω_3 axis. Although this axis is the one for which the projection-slice theorem is best able to correct the phasing error, it is also the one for which the phase error is most likely to be largest because of the difficulties that can arise in accurately determining the zero delay between the third pulse and the local oscillator, especially in spectrometers where the local oscillator does not travel through the sample and is overlapped with the signal after the sample. The qualitative effects of placing the phase error on the ω_1 axis are the same, just with a different dependence on the frequency.

Figure 4(a) shows the CLS (red) and IvCLS (black) analyses for a phasing error corresponding to a group delay of $\Delta t = 1$ fs (triangles) with the analyses for no phase error shown for comparison. In both cases, the effects of the phasing error are modest. For the IvCLS, there is essentially no effect due to the phasing error. Both the amplitudes of the decay components and the time constant remain unchanged. In the case of the
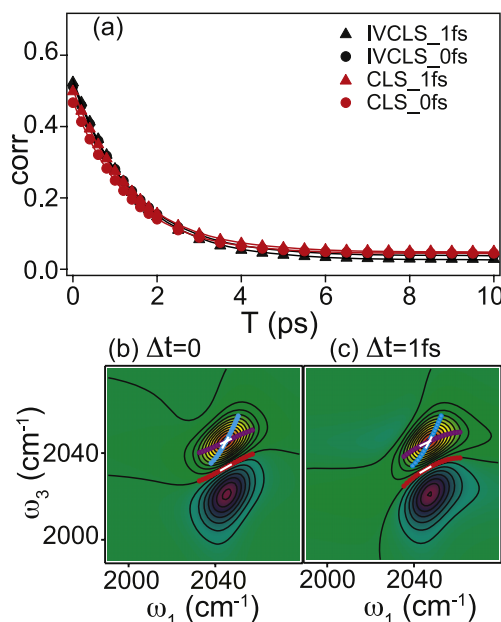

FIG. 4. Phasing error effects on (a) IvCLS and CLS methods. Simulated 2D IR spectra for a waiting time of 0 fs with 0 fs (b) and 1 fs (c) phasing errors, respectively. The purple, blue, and red dots represent the centerline, inverse centerline, and nodal line, respectively, and the white solid lines are the corresponding linear fits.

TABLE IV. Single exponential fit parameters for CLS, ELP, 2DGC, IvCLS, and NLS analyses of simulated data with a phasing error on ω_3 of the form $\exp(i \cdot \Delta t \cdot 2\pi \cdot c \cdot \omega_3)$.

Analysis method	Δt/fs	A_1	τ/fs	A_2
CLS	0	0.43	1400	0.044
	1	0.46	1400	0.048
ELP	0	0.48	1400	0.037
	1	0.51	1400	0.026
2DGC	0	0.53	1500	0.046
	1	0.58	1500	0.048
IvCLS	0	0.52	1400	0.051
	1	0.53	1400	0.053
NLS	0	0.50	1400	0.048
	1	0.54	1300	0.050

CLS method, however, the time constant remains unchanged but the amplitudes of both the decay and the offset increase somewhat. These increases are reflective of the effects that the phasing error has on the lineshape. Figures 4(b) and 4(c) show spectra for 0 fs and 1 fs phasing error, respectively, along with the analyses for the IvCLS, CLS, and NLS (Table IV). As is clearly evident, the phasing error causes a twist in the lineshape that leads to curvature of the centerlines and the nodal line. In addition, the peak position shifts somewhat. The major consequence of these effects is that the analysis of the lineshapes becomes inherently uncertain. Because of the curvature of the lineshape, the results of the analyses are necessarily different depending on the region over which we do the linear fit to determine the slope. Both the choice of width and position for this fit can significantly affect the results of the analysis. For the results shown in Figure 4, we have retained the same fit region for the analysis of the spectra with the phase error included as for the spectra with no phasing error, which is centered on the peak of the spectrum without phasing error. Choosing a region centered on the new peak position after including the phasing error decreases the magnitude of the effect on the peak amplitude but changes the time constant of the decay (data not shown).

For all of the other analysis methods, the effects of the phasing error are somewhat more significant. The NLS analysis (see supplementary material[44]) exhibits an effect similar to the CLS except that the time constant decreases slightly. The ELP and 2DGC analyses (also shown in the supplementary material[44]) show no change in the time constants but exhibit somewhat larger effects on the amplitudes. In the case of the 2DGC, both the amplitude and offset increase by about 10% or less. In the case of the ELP, however, while the amplitude of the decay increases somewhat, the amplitude of the offset decreases by 30%. The 2DGC and the ELP experience larger effects resulting from the phasing error because of the differing ways that they reflect the lineshape compared to the other methods. The 2DGC has some flexibility given that it involves a Gaussian fit to the lineshape, but the phase twisted lineshape is no longer well approximated as a Gaussian. For the ELP, the phasing error causes the antidiagonal width to be frequency dependent as a result of the phase twist, and this effect distorts the amplitude of the ellipticity. Thus, the ELP and 2DGC

methods are less well suited than the others for analyzing lineshapes with potential phasing errors.

D. Signal-to-noise effects

To study the effects of apodization, anharmonicity, and phasing errors on the line shape analysis methods, we have used simulated data, which have the advantage of known FFCF parameters and nearly infinite S/N. Real experimental data, however, always have finite S/N and the noise contributions can have a significant effect on the lineshape and methods to extract information about the loss of frequency correlation. The early experiments involving 2D IR spectroscopy to measure the dynamics of solvents and proteins involved systems with strong chromophores at relatively high concentrations so that the 2D IR signal was quite strong and the S/N high.[8,9,12,20,43] Increasingly, however, researchers are pursuing experiments involving weaker chromophores and targets, such as proteins, for which aqueous solubility is limited. In such systems, even significant amounts of signal averaging can yield modest S/N and leave the line shape distorted by the noise. It is essential that the analysis method used to extract the frequency correlation information from the data be robust to the effects of noise. Thus, an understanding of the relative strengths of these methods for data with low S/N is an important new insight.

To assess the effects of noise, we use azide in D_2O, which has previously been studied by photon echo spectroscopy,[9] as an illustrative example. We collected high S/N data by signal averaging between 50 and 2400 scans depending on the waiting time and took the data from a single pulse shaper scan for the low S/N data. We collected and analyzed four replicates to establish reliable statistics for the results. Figure 5 shows the analysis results for the high (a) and low (b) S/N data using the IvCLS (blue), ELP (black), 2DGC (green), and CLS (red) analysis methods. Each point is an average of the four analyses for four independent measurements at that waiting time, and the standard deviation of the individual analyses is used as a weighting coefficient for the exponential fit, which is shown as solid lines. In addition, representative spectra are also shown for the high (average S/N = 250) (c) and low (average S/N = 27) (d) S/N measurements for a waiting time of T = 1000 fs. For better comparison of the S/N of the spectra, we have normalized each spectrum to the maximum of the 0-1 transition and display 11 equally spaced contour levels from -1 to 1. To quantify the S/N of the spectra, we calculate the RMS noise of a spectral area enclosed by ω_3 = 2070–2085 cm^{-1} and ω_1 = 2004–2015 cm^{-1}, and we use the difference in amplitudes of the oppositely signed 0-1 and 1-2 transitions as a measure of the signal.

A minor complicating feature of this experimental system is that the azide antisymmetric stretching transition, which is centered at approximately 2045 cm^{-1}, is located on the low-frequency tail of the O–D stretching transition of D_2O. As a result, a solvent background associated with this O–D stretching vibration overlaps with the spectral response from azide. Fortunately, the O–D stretching response decays rapidly compared the decay of the azide response. Thus, we only analyze the data for waiting times greater than or equal to 500 fs for which the solvent background is substantially

TABLE V. Single exponential fit parameters for analyses of azide in D_2O data.

Analysis method	S/N	A_1	τ/fs	A_2
CLS	27	0.49 ± 0.08	1000 ± 400	0 ± 0.08
	250	0.52 ± 0.01	800 ± 200	0.01 ± 0.01
ELP	27	0.41 ± 0.08	700 ± 500	0 ± 0.06
	250	0.34 ± 0.02	800 ± 400	0.03 ± 0.02
2DGC	27	...	...	...
	250	0.51 ± 0.01	1100 ± 200	0.03 ± 0.01
IvCLS	27	...	...	...
	250	0.66 ± 0.01	1100 ± 200	0 ± 0.01
NLS	27	...	...	...
	250	0.64 ± 0.02	1200 ± 200	0 ± 0.02

weaker than the azide signal. Nevertheless, some evidence of the solvent background remains in the spectrum as is seen clearly in the additional contributions along the diagonal in Figure 5(c). This background affects the lineshape analysis methods and contributes to some of the scatter in the points at early waiting times and increases the uncertainty in the fit parameters, especially for the ELP method, which appears to be more sensitive to this background response.
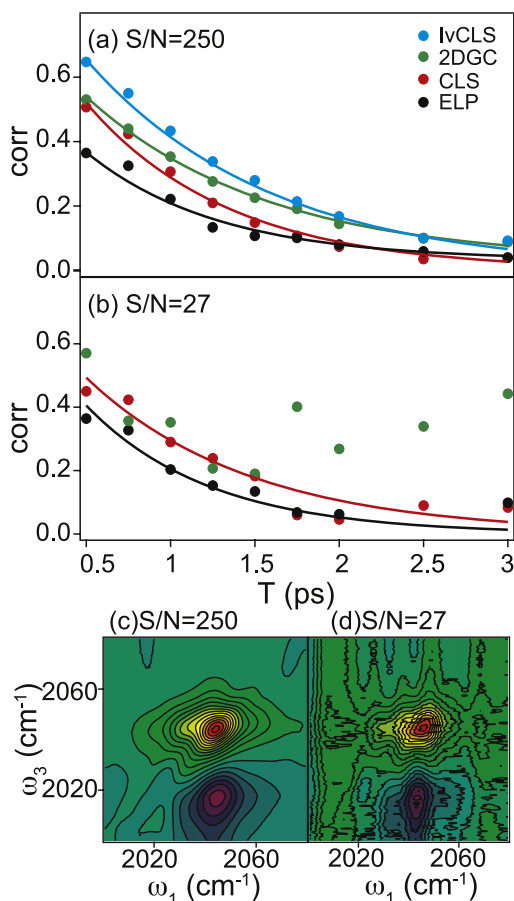

FIG. 5. IvCLS (blue), ELP (black), 2DGC (green), and CLS (red) analyses of high S/N (a) and low S/N (b) 2D IR spectra of azide anion in D_2O. Each point is the average of the analysis from 4 independent 2D IR measurements. The solid lines are the exponential fits to the data points. Panels (c) and (d) show representative 2D IR spectra for a waiting time of 1000 fs from the high and low S/N data sets, respectively.

At high S/N, all of the analysis methods give reasonable correlation decays with time constants that are consistent with one another and with previous results from the Hochstrasser group (Table V). The covariance between the offset and the time constant causes the decay time to be somewhat shorter and the offset somewhat smaller for the fit than might be expected from the previous echo measurements, but these values are, nevertheless, in reasonable agreement with the previous study. At low signal to noise, however, the different analysis methods respond to the poorer S/N differently and, in some cases, become so unstable as to be unable to fit to a decay.

For the IvCLS analysis, the results are completely unstable at low S/N to the point that most of the values are unphysical lying outside of the range of allowed values between 0 and 1 (data not shown). The major contributing factors to this result are the difference in the characteristics of the noise in the two frequency dimensions for our apparatus and the difference in step size for the two axes. Because we collect the signal in ω_3 using an array detector, the noise in the ω_3 dimension is correlated. Consequently, the noise is dominated by vertical banding in the 2D IR spectrum as can easily be seen in Figure 5(d). In addition, the frequency step size in ω_1 is larger than that in ω_3 because of the high pixel density of our CMOS array, so the spectrum is significantly oversampled in the ω_3 axis and is smoother in that dimension. As a result of these features, the centerline from the IvCLS analysis exhibits discontinuities as seen in Figure 6, which shows the 2D IR spectrum from the low S/N azide in D_2O for a waiting time of 500 fs zoomed in on the 0-1 transition. The blue markers show the centerline constructed as described for the IvCLS method, i.e., each represents the location of the maximum in ω_1 for a fixed value of ω_3. The points fall in groups because the larger step size in ω_1 means that the spectrum is not as smooth in this coordinate and so the location of the maximum in ω_1 will jump as the value of ω_3 changes. The vertical banding of the noise exacerbates this problem because the variations in intensity are greatest along the ω_1 axis, whereas they are correlated for the values of ω_3. These discontinuities lead to instabilities in the value of the slope of the centerline, which makes this method unsuitable for data from our apparatus. These features of the data are particular to our apparatus, though it may well be the case that other researchers will encounter similar problems as most approaches for collecting 2D IR spectra employ an array detector, which will lead to noise correlations in the
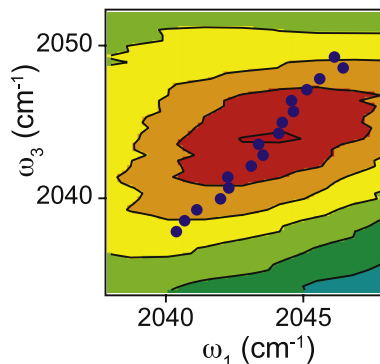

FIG. 6. Inverse centerline (blue markers) for the spectrum of low S/N azide anion in D_2O at T = 500 fs.
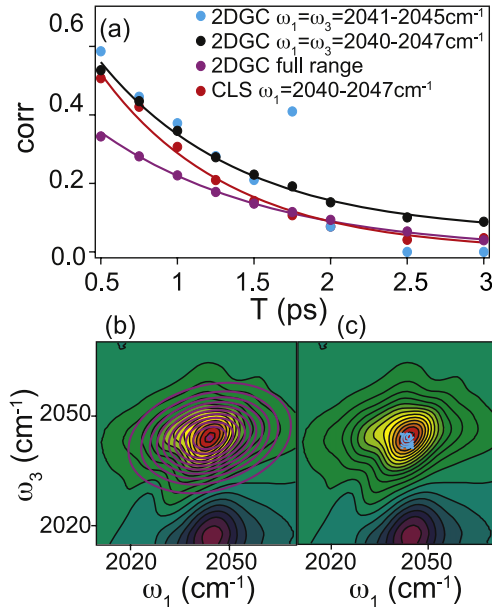
TABLE VI. Single exponential fit parameters for CLS and 2DGC analyses of high S/N azide in D_2O data.

Analysis method	Fitting range	A_1	τ/fs	A_2
CLS	$\omega_1 = 2040–2047$	0.52 ± 0.01	800 ± 200	0 ± 0.01
2DGC	$\omega_1 = \omega_3 = 2041–2045$	...	...	...
	$\omega_1 = \omega_3 = 2040–2047$	0.51 ± 0.01	1100 ± 200	0.03 ± 0.01
	Full range	0.35 ± 0.2	1000 ± 2000	0 ± 0.2

FIG. 7. (a) Comparison of the CLS (red) and 2DGC analyses for an unconstrained 2DGC fit (purple) and a 2DGC fit constrained to a small area near the center of the peak (blue). Examples of the unconstrained and constrained Gaussian fits are shown in panels (b) and (c), respectively.

ω_3 axis. Nevertheless, these problems may be less severe in other circumstances, especially for the lower pixel densities for MCT array detectors, so the quality of this method should be evaluated on a system-by-system basis.

For the experimental data with low S/N, the NLS (see supplementary material[44]) and the 2DGC (Figure 5) analyses also become unstable. The 2DGC method requires well-defined edges of the line shape to fit the data and there are more points around the edges of the data than in the center. Because the noise affects the points near the edges of the lineshape more than the points in the center and there are more points around the edges, the noise has a more significant effect for the 2DGC method than for the CLS, which focuses on the central parts of the lineshape where the signal is maximized. One potential solution to this problem, for the 2DGC method, is to restrict the fit to a smaller fitting range near the center of the peak. Figure 7 illustrates the effects of such an analysis. Figure 7(a) shows the comparison between the CLS analysis at high S/N (red) and three analyses of the high S/N data using the 2DGC method, one where the Gaussian is fit to the entire 0-1 peak (purple), another where the fit is constrained to a small portion of the peak in the center from 2040 to 2047 cm^{-1} (black), and a third where the fit is constrained to an even smaller region from 2041 to 2045 cm^{-1} in both axes (blue) (Table VI). Representative 2D IR spectra are shown in Figure 7 with the full fit in panel (b) and the most constrained fit in panel (c). Clearly, the constrained fit focuses on a much smaller region where the signal is largest, which reduces the impact of the background noise on the fit, but it will also reduce the information content of the fit as the sampled region is much smaller and reflects less of the frequency correlation. Comparing the 2DGC results to the results at high S/N shown in panel (a), the constrained results are more consistent with the results of the CLS decay, but the most constrained region becomes unstable as evidenced

by the points that fall far from the decay. This approach can improve the robustness of the 2DGC method to noise, but its effectiveness is limited based on the level of constraint required and the instabilities that will inevitably result from a fitting area that is too small and contains too little spectral information. Ultimately, this approach is unable to overcome the impacts of the noise at low S/N, and the 2DGC method exhibits essentially no decay as seen in Figure 5(b) (green).

The best alternative to the CLS method is the ELP analysis. At high S/N, the ELP and CLS have the same time constant, but the amplitude of the decay for the ELP is less than that for the CLS by about 30%. At low S/N, the time constant for the ELP decreases somewhat, though the effect of S/N on the amplitudes is only minor. Thus, the ELP remains rather robust to S/N. It is worth noting that the uncertainty in the parameters for the ELP is greater than that for the CLS even at high S/N as a result of the greater scatter of the points in the decay. This is likely a result of the fact that like the 2DGC, the ELP results from fitting the lineshape and is somewhat more affected by the noise at the edges of the data than the CLS is. Nevertheless, this effect is much less significant for the ELP than for the 2DGC, and the ELP remains almost as good of a representation of the correlation decay as the CLS at both high and low S/N.

IV. CONCLUSION

We have compared the effects of frequently encountered experimental challenges on five different methods for analyzing 2D IR data to extract the FFCF. Although all of the methods we have tested can be quickly and easily obtained from the experimental data, they may lead to very different conclusions depending on the characteristics of the system of interest and the quality of the data. Using simulated data with varying apodization, we showed that the IvCLS and 2DGC are most robust to changing the apodization time and function, but that for the CLS, ELP, and NLS, the time constants and relative amplitudes for the decay are conserved even though the absolute amplitudes decrease with decreasing apodization time. Simulated spectra with varying anharmonicities show that the IvCLS and 2DGC methods become unstable when the anharmonicity becomes too small, but the NLS method becomes unstable when the anharmonicity is too large. The CLS and ELP methods show no effects from varying the anharmonicity. For data in which phasing error introduces a phase twisted lineshape, the effects of the phase twist are small to negligible for the CLS and IvCLS but more significant for the other methods. Finally, using experimental measurements of azide

in D_2O, we show that all of the methods work well at high S/N but that the IvCLS, NLS, and 2DGC become unstable at low S/N. Taken together, these results suggest that the CLS method will, for most cases, offer the best analysis of the experimentally measured spectral diffusion dynamics. Because the magnitude of the CLS depends on the apodization, it is critical that the apodization time remains constant for all waiting times. Nevertheless, the exact value of the apodization time is not critical as the relative amplitudes and time constants remain unaffected so long as the amplitudes of the components of the correlation decay are large enough to be out of the experimental uncertainty in the data.

ACKNOWLEDGMENTS

[1]P. Hamm and M. T. Zanni, *Concepts and Methods of 2D Infrared Spectroscopy* (Cambridge University Press, New York, NY, 2011).

[2]S. Bagchi, S. G. Boxer, and M. D. Fayer, J. Phys. Chem. B **116**, 4034 (2012).

[3]A. Tokmakoff, Science **317**, 54 (2007).

[4]D. B. Wong, C. H. Giammanco, E. E. Fenn, and M. D. Fayer, J. Phys. Chem. B **117**, 623 (2012).

[5]J. J. Loparo, S. T. Roberts, and A. Tokmakoff, J. Chem. Phys. **125**, 194522 (2006).

[6]J. B. Asbury, T. Steinel, C. Stromberg, S. A. Corcelli, C. P. Lawrence, J. L. Skinner, and M. D. Fayer, J. Phys. Chem. A **108**, 1107 (2004).

[7]Y. S. Kim and R. M. Hochstrasser, J. Phys. Chem. B **113**, 8231 (2009).

[8]M. F. Decamp, L. Deflores, J. M. McCracken, A. Tokmakoff, K. Kwac, and M. Cho, J. Phys. Chem. B **109**, 11016 (2005).

[9]P. Hamm, M. Lim, and R. M. Hochstrasser, Phys. Rev. Lett. **81**, 5326 (1998).

[10]J. D. Eaves, J. J. Loparo, C. J. Fecko, S. T. Roberts, A. Tokmakoff, and P. L. Geissler, Proc. Natl. Acad. Sci. U.S.A. **102**, 13019 (2005).

[11]N. Demirdöven, M. Khalil, and A. Tokmakoff, Phys. Rev. Lett. **89**, 237401 (2002).

[12]M. W. Nydegger, S. Dutta, and C. M. Cheatum, J. Chem. Phys. **133**, 134506 (2010).

[13]S. Dutta, W. Rock, R. J. Cook, A. Kohen, and C. M. Cheatum, J. Chem. Phys. **135**, 055106 (2011).

[14]R. Bloem, K. Koziol, S. A. Waldauer, B. Buchli, R. Walser, B. Samatanga, I. Jelesarov, and P. Hamm, J. Phys. Chem. B **116**, 13705 (2012).

[15]D. B. Strasfeld, Y. L. Ling, S.-H. Shim, and M. T. Zanni, J. Am. Chem. Soc. **130**, 6698 (2008).

[16]S.-H. Shim, R. Gupta, Y. L. Ling, D. B. Strasfeld, D. P. Raleigh, and M. T. Zanni, Proc. Natl. Acad. Sci. U.S.A. **106**, 6614 (2009).

[17]C. T. Middleton, P. Marek, P. Cao, C.-C. Chiu, S. Singh, A. M. Woys, J. J. de Pablo, D. P. Raleigh, and M. T. Zanni, Nat. Chem. **4**, 355 (2012).

[18]A. Remorino, I. V. Korendovych, Y. Wu, W. F. Degrado, and R. M. Hochstrasser, Science **332**, 1206 (2011).

[19]M. C. Thielges, J. K. Chung, J. Y. Axup, and M. D. Fayer, Biochemistry **50**, 5799 (2011).

[20]J. R. Hill, D. D. Dlott, C. W. Rella, T. I. Smith, H. A. Schwettman, K. A. Peterson, A. Kwok, K. D. Rector, and M. D. Fayer, Biospectroscopy **2**, 277 (1996).

[21]H. S. Chung, Z. Ganim, K. C. Jones, and A. Tokmakoff, Proc. Natl. Acad. Sci. U.S.A. **104**, 14237 (2007).

[22]A. Ghosh, J. Qiu, W. F. Degrado, and R. M. Hochstrasser, Proc. Natl. Acad. Sci. U.S.A. **108**, 6115 (2011).

[23]M. Koziński, S. Garrett-Roe, and P. Hamm, J. Phys. Chem. B **112**, 7645 (2008).

[24]D. G. Kuroda, J. D. Bauman, J. R. Challa, D. Patel, T. Troxler, K. Das, E. Arnold, and R. M. Hochstrasser, Nat. Chem. **5**, 174 (2013).

[25]J. N. Bandaria, S. Dutta, M. W. Nydegger, W. Rock, A. Kohen, and C. M. Cheatum, Proc. Natl. Acad. Sci. U.S.A. **107**, 17974 (2010).

[26]S. Dutta, Y.-L. Li, W. Rock, J. C. D. Houtman, A. Kohen, and C. M. Cheatum, J. Phys. Chem. B **116**, 542 (2011).

[27]W. Rock, Y.-L. Li, P. Pagano, and C. M. Cheatum, J. Phys. Chem. A **117**, 6073 (2013).

[28]N. Simpson, D. J. Shaw, P. W. J. M. Frederix, A. H. Gillies, K. Adamczyk, G. M. Greetham, M. Towrie, A. W. Parker, P. A. Hoskisson, and N. T. Hunt, J. Phys. Chem. B **117**, 16468 (2013).

[29]H. Ishikawa, I. J. Finkelstein, S. Kim, K. Kwak, J. K. Chung, K. Wakasugi, A. M. Massari, and M. D. Fayer, Proc. Natl. Acad. Sci. U.S.A. **104**, 16116 (2007).

[30]A. T. Krummel, P. Mukherjee, and M. T. Zanni, J. Phys. Chem. B **107**, 9165 (2003).

[31]A. T. Krummel and M. T. Zanni, J. Phys. Chem. B **110**, 13991 (2006).

[32]K. Kwac and M. Cho, J. Chem. Phys. **119**, 2256 (2003).

[33]K. Lazonder, M. S. Pshenichnikov, and D. A. Wiersma, Opt. Lett. **31**, 3354 (2006).

[34]S. T. Roberts, J. J. Loparo, and A. Tokmakoff, J. Chem. Phys. **125**, 084502 (2006).

[35]K. Kwak, S. Park, I. J. Finkelstein, and M. D. Fayer, J. Chem. Phys. **127**, 124503 (2007).

[36]K. Kwak, D. E. Rosenfeld, and M. D. Fayer, J. Chem. Phys. **128**, 204505 (2008).

[37]M. Candelaresi, A. Gumiero, K. Adamczyk, K. Robb, C. Bellota-Anton, V. Sangal, J. Munnoch, G. M. Greetham, M. Towrie, P. A. Hoskisson, A. W. Parker, N. P. Tucker, M. A. Walsh, and N. T. Hunt, Org. Biomol. Chem. **11**, 7778 (2013).

[38]K. Kwac and M. Cho, J. Phys. Chem. A **107**, 5903 (2003).

[39]J. D. Hybl, A. Yu, D. A. Farrow, and D. M. Jonas, J. Phys. Chem. A **106**, 7651 (2002).

[40]S.-H. Shim, D. B. Strasfeld, Y. L. Ling, and M. T. Zanni, Proc. Natl. Acad. Sci. U.S.A. **104**, 14197 (2007).

[41]E. H. G. Backus, S. Garrett-Roe, and P. Hamm, Opt. Lett. **33**, 2665 (2008).

[42]R. Kubo, in *Advances in Chemical Physics* (John Wiley & Sons, Inc., 2007), p. 101.

[43]M. W. Nydegger, W. Rock, and C. M. Cheatum, Phys. Chem. Chem. Phys. **13**, 6098 (2011).

[44]See supplementary material at http://dx.doi.org/10.1063/1.4918350 for supporting figures and tables referenced in the main text.